Journal of Power Sources 296 (2015) 383–391

Contents lists available at ScienceDirect

Journal of Power Sources

journal homepage: www.elsevier.com/locate/jpowsour

Energy awareness for supercapacitors using Kalman filter state-of-charge tracking☆,☆☆

Andrew Nadeau*, Moeen Hassanalieragh, Gaurav Sharma, Tolga Soyata

Dept. of Electrical & Computer Engineering, University of Rochester, PO Box 270126, Rochester, NY 14627-0126, USA

HIGHLIGHTS

- The energy stored in a supercapacitor cannot be determined by terminal voltage alone.
- Kalman state tracking with a three branch model improves stored energy awareness.
- A novel estimation technique enables in-situ estimation of required model parameters.
- The proposed method accurately determines the energy buffered in a supercapacitor.

ARTICLE INFO

Article history:
Received 7 May 2015
Received in revised form
10 July 2015
Accepted 16 July 2015
Available online xxx

Keywords:
Supercapacitor
Three branch model
State of charge
Parameter estimation
Kalman
Energy awareness

ABSTRACT

Among energy buffering alternatives, supercapacitors can provide unmatched efficiency and durability. Additionally, the direct relation between a supercapacitor's terminal voltage and stored energy can improve energy awareness. However, a simple capacitive approximation cannot adequately represent the stored energy in a supercapacitor. It is shown that the three branch equivalent circuit model provides more accurate energy awareness. This equivalent circuit uses three capacitances and associated resistances to represent the supercapacitor's internal SOC (state-of-charge). However, the SOC cannot be determined from one observation of the terminal voltage, and must be tracked over time using inexact measurements. We present: 1) a Kalman filtering solution for tracking the SOC; 2) an on-line system identification procedure to efficiently estimate the equivalent circuit's parameters; and 3) experimental validation of both parameter estimation and SOC tracking for 5 F, 10 F, 50 F, and 350 F supercapacitors. Validation is done within the operating range of a solar powered application and the associated power variability due to energy harvesting. The proposed techniques are benchmarked against the simple capacitive model and prior parameter estimation techniques, and provide a 67% reduction in root-mean-square error for predicting usable buffered energy.

1. Introduction

Supercapacitors represent an emerging and rapidly developing energy storage technology that provides significant robustness and efficiency benefits over alternative energy storage technologies [2]. In particular, compared with electrochemical batteries, supercapacitors can typically survive 100 to 1000 times as many charge–discharge cycles before there is significant degradation of capacity or efficiency [3]. This is a substantial benefit for remote systems because it can reduce the frequency of maintenance visits to remotely deployed nodes and thereby achieve greater cost-effectiveness. Thus far, supercapacitors have been commonly applied for buffering energy over short durations, e. g. supercapacitor-battery hybrid storage [4,5], and regenerative breaking [6–8]. For these applications, peak power and short-term efficiency are supercapacitors' most important strengths.

The proposed work targets long-term energy storage applications where accurate energy awareness is important. For example, a remotely deployed system can rely on solar energy harvesting. Without a reliable connection to the electrical grid, accurate

☆ This work was supported in part by the National Science Foundation grant CNS-1239423.

☆☆ A preliminary version of this paper was presented at IEEE Intl. Conf. on Acoustics Speech and Sig. Proc. (ICASSP 2014), Florence, Italy, 2014 [1].

* Corresponding author.
E-mail addresses: andrew.nadeau@rochester.edu (A. Nadeau), m.hassanalieragh@rochester.edu (M. Hassanalieragh), gaurav.sharma@rochester.edu (G. Sharma), tolga.soyata@rochester.edu (T. Soyata).

http://dx.doi.org/10.1016/j.jpowsour.2015.07.050
0378-7753/

knowledge of a supercapacitor's SOC (state-of-charge) is critical to know how much energy remains available to the system [9,10]. Long-term energy storage applications are also motivated by the robustness and durability benefits of supercapacitors. These benefits have been used to prototype a supercapacitor-based, WSN (wireless sensor node) with 20 years of projected service-free lifetime [11].

Tracking SOC can also be important when supercapacitors are used in banks of multiple devices in series or parallel configurations. These configurations benefit from load balancing in order to prevent specific cells from over-charging and suffering premature capacity degradation [12]. However, if SOC is not accounted for it can be difficult to perform on-line measurements of capacity degradation for the individual cells, or make real-time load balancing decisions.

Kalman tracking for a supercapacitor's SOC is proposed to exploit the energy awareness benefits of supercapacitors. Compared to rechargeable batteries, the stored energy in a supercapacitor is more directly related to its terminal voltage, v_{sc}, via the capacitance, C. However, the simple model, $Cv_{sc}^2/2$, for stored energy neglects important non-ideal behavior: both charge redistribution and leakage affect storage capacity and the net portion of the energy that is available to a system after internal losses. It is shown that the total energy needed to fully charge a supercapacitor to its maximum voltage can vary up to 23% depending on the power level at which a supercapacitor is charged. This variation in capacity cannot be accounted for by the simple model. Extensive work has been done to model supercapacitor behavior [13–21], but this paper goes to the next step: translating these models into usable energy awareness. The proposed Kalman tracking technique uses the three branch equivalent circuit [15] to account for this non-ideal capacity variability. The Kalman filter balances uncertainty by weighting the correction due to each new observation on the estimate of the circuit's SOC.

A common difficulty of Kalman tracking is the accuracy of the model. The parameter estimation technique proposed here provides a novel method to fit the parameters of the three branch equivalent circuit. The proposed technique does not require specific tests to be performed in the field or before the device is deployed: fitting is able to utilize the actual current profiles encountered by the application, provided significant power variability occurs. Prior methods for parameter estimation have relied on electrochemical impedance spectroscopy (EIS), which requires specialized test equipment and cannot be performed in the field [22–24], or have been designed to only fit the capacitance and series resistance, but not the parameters for redistribution [25].

In addition to describing the proposed parameter estimation technique and Kalman tracking methodology, this paper also presents experimental validation of both techniques for 50 F supercapacitors and parameter estimation for 5 F, 10 F and 350 F supercapacitors.

This paper begins with background and modeling for supercapacitors in Section 2. Sections 3 and 4 then present the proposed parameter estimation and Kalman tracking techniques. Section 5 evaluates the performance of each technique as compared to the simple capacitive model. Results and discussion of the experiments are given in Section 6. Conclusions and contributions are summarized in Section 7.

2. Modeling

Charge storage in supercapacitors relies primarily on two phenomena: the EDL (electric double layer) and pseudocapacitance [13], that are illustrated in Fig. 1a. Voltage applied across the supercapacitor terminals pushes charge to the surface of the electrode material forming a surface layer. Oppositely charged ions in the electrolyte are, in turn, attracted by the surface charge forming a second layer. The two layers make up the EDL capacitance. Reversible chemical reactions store additional charge on the surface of the electrodes and contribute pseudocapacitance. Much higher capacitances than conventional electrolytic devices are obtained because of the small distance (comparable to atomic radii) between opposite charges and the large surface area of the porous electrodes.

A simple capacitive model fails to account for three sources of non-ideal behavior in supercapacitors: both the EDL and pseudocapacitance are voltage dependent; the diffusion of ions into the porous materials is not instantaneous; and there is spontaneous leakage of stored charge. Diffusion, or charge redistribution, is observable after a charging current into a supercapacitor is discontinued. Diffusion of ions in the electrolyte causes the terminal voltage, v_{sc}, to spontaneously decay. Diffusion push ions away from regions of high concentration near the readily accessible (and more quickly charged) portions of the porous surface. Modeling a supercapacitor's SOC accounts for charge redistribution as the penetration of stored charge into a string of resistive-capacitive (RC) transmission line storage elements [14] as in Fig. 1a, or simplified as an array of time constants in parallel RC branches [15] as in Fig. 1b. Leakage has been simply modeled as a fixed parallel resistance [15], or a variable resistance depending on factors such as the supercapacitor's voltage, temperature and internal state [16,26,17,18,27].

Prior work has shown that a simple capacitive model can provide adequate energy awareness for low powered solar-supercapacitor WSN (wireless sensor nodes) [28,29]. Online parameter estimation has also been demonstrated for a single branch model [30]. Although the simple model is preferable because of the limited computational capabilities of these systems, results in Ref. [29] show significant improvement when the fixed capacitance, C_{simple}, is tuned to the specific discharge speed, similar to the manner in which three branch equivalent circuit intrinsically accounts for the effect of charging speed on SOC. Modeling a supercapacitor using the three branch equivalent circuit is especially important for higher powered systems with greater power variability than WSN.

The impact of both redistribution and leakage when the charging current, i_{sc}, is varied over a wider range of power is shown in Fig. 2. The observed supercapacitor behavior is compared to the baseline, simple capacitive model for stored energy,

$$E = \frac{1}{2} C_{simple} v_{sc}^2, \tag{1}$$

where v_{sc} is the terminal voltage for the supercapacitor, and the capacitance, C_{simple}, is fitted to the average slope of the observed data,

$$C_{simple} = \left(\frac{1}{N} \sum_{n=1}^{N} \frac{dv_{sc}}{dq} \right)^{-1}. \tag{2}$$

For each of the N observations in (2), taken over the three durations of charging in Fig. 2, the differential charge, dq, is calculated as $i_{sc}dt$, where i_{sc} denotes the (constant) charging current and t denotes time. In terms of energy awareness, Fig. 2 shows that the total energy needed to charge the 50 F supercapacitor,

$$E_{obs} = \int v_{sc} i_{sc} dt = \int v_{sc} dq, \tag{3}$$

varies between 188 J and 231 J (23% variation) even though the

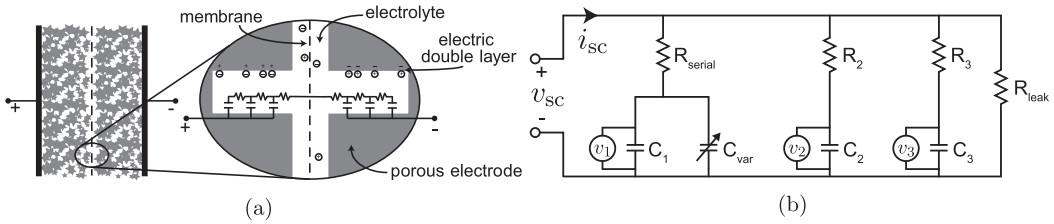

Fig. 1. As shown in (a), each of a supercapacitor's terminals is connected to a porous electrode material such as activated carbon. The conductive electrodes are immersed in an electrolyte but separated by a membrane which only allows the ions in the electrolyte to pass through. Diffusion of the ions into the porous surface is modeled by the three branch equivalent circuit [15], shown in (b). Each branch has a time constant of increasing duration, $R_{serial}\ C_1 < R_2\ C_2 < R_3\ C_3$, modeling initial, intermediate, and long term behavior.

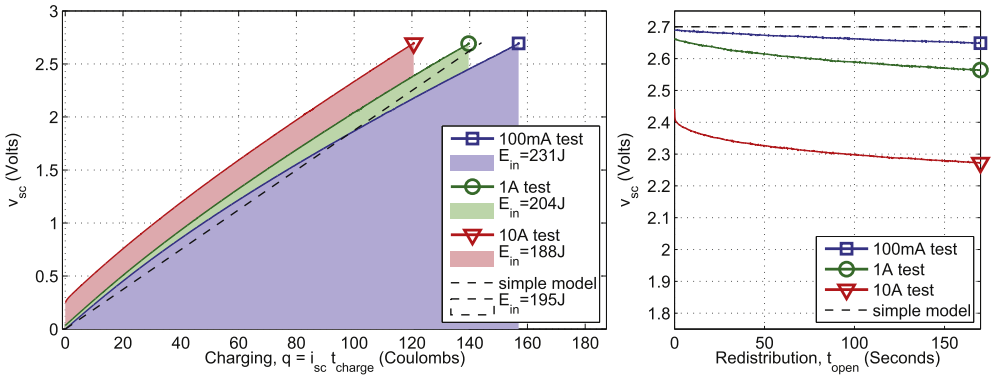

Fig. 2. *Charging*, on the left, shows the terminal voltage of a 50 F *Maxwell Boostcap Ultracapacitor* as it is charged with 100 mA, 1 A, and 10 A constant currents. Because *Charging* is scaled to Coulombs, q, it is easy to see that a supercapacitor does not strictly follow the proportion, $v_{sc} = 1/C \cdot q$, predicted by the simple model. The supercapacitor always starts in a completely discharged state, and current, i_{sc}, is disconnected when v_{sc} reaches the device's rated voltage, 2.7 V. *Redistribution*, on the right, shows v_{sc} starting at $t_{open} = 0$ s when i_{sc} is first disconnected.

supercapacitor is charged to the same terminal voltage, and only the charging current, i_{sc}, is varied. For a 350 F supercapacitor, the measured value of E_{obs} varies from 1.18 kJ to 1.31 kJ (11% variation) despite the proportionally smaller range of charging currents tested for the larger supercapacitor. Redistribution predicts this variation in charge storage because the storage capacity of the supercapacitor's porous electrode surfaces is more fully accessed over the longer duration of charging for the lower currents. *Redistribution* in Fig. 2 shows that the decline in v_{sc} after charging stops is proportional to the speed of charging.

The proposed Kalman technique uses a simple fixed resistance to model leakage, and focuses on tracking the supercapacitor's SOC due to redistribution using the three branch equivalent circuit [15]. The real world implications of tracking a supercapacitor's SOC are motivated by the power variability shown in Fig. 3, for a system using supercapacitors to buffer solar energy harvesting. Other work [31,32] has applied battery modeling to supercapacitors. However, supercapacitors do not require the complexity of these models devoted to modeling hysteresis and the nonlinear relationship between a battery's terminal voltage and SOC. For predicting short-term supercapacitor performance, it is beneficial to use more detailed models such as the transmission line elements in Fig. 1a that are accurate over much wider frequency ranges and tuned using electrochemical impedance spectroscopy [22,23,33]. For our target applications the three branch equivalent circuit provides a good balance between accuracy, complexity, and the ability to use on-line parameter estimation. Prior work has used the three branch equivalent circuit to model charge redistribution [34], but this method did not consider SOC tracking or on-line parameter estimation.

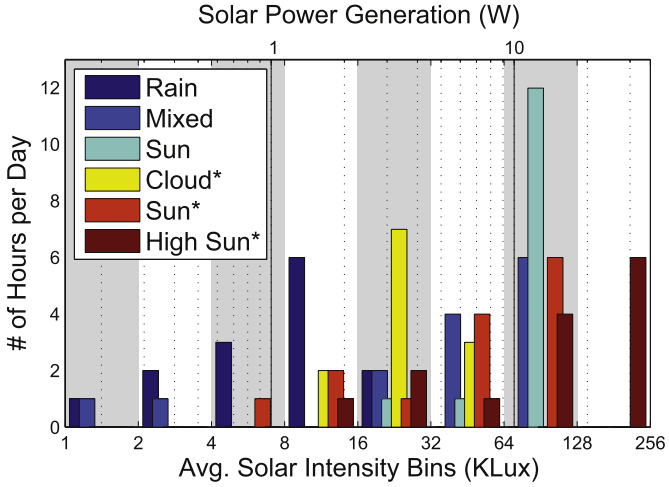

Fig. 3. The histogram of solar generation from 21 *RadioShack 1.5 W* panels (max. 31.5 W at 200 KLux) varies by two orders-of-magnitude, resulting in significant potential for non-ideal supercapacitor behavior while buffering the energy. The marked data (*) is recorded in Italy [35], whereas the rest of the days are measured in Rochester NY, USA [10].

3. Parameter estimation method

Estimating the parameters of the three branch equivalent circuit is nontrivial due to the fact that the internal state is not observable. Linear LMSE (least mean square error) fitting is proposed for parameter identification because i_{sc} in the three branch equivalent circuit in Fig. 1b can be fitted as a linear combination of the branch currents,

$$i_{sc} = C_1\frac{dv_{sc}}{dt} + C_{var}v_{sc}\frac{dv_{sc}}{dt} + \frac{1}{R_2}(v_{sc} - v_2) + \frac{1}{R_3}(v_{sc} - v_3), \quad (4)$$

where C_1 and $C_{var}v_{sc}$ are the fixed and voltage dependent capacitances included in the first branch and, R_2, R_3 and v_2, v_3 are the resistances and voltages in the second and third branches, each as labeled in Fig. 1b. Leakage is neglected as it is much less significant than redistribution in the short term.

The first and second terms in (4), accurately approximate the current in the first branch using the observable slope of v_{sc} rather than the true slope of hidden voltage, v_1. This is a safe assumption because the voltage drop between v_{sc} and v_1 due to R_{serial} is small. Jumps in v_{sc} when i_{sc} switches on or off are omitted in order to avoid the discontinuities in dv_{sc}/dt. The last two terms in (4), for the current from the second and third branches, depend on the low pass filtered branch voltages, v_2 and v_3, with time constants, τ_2 and τ_3,

$$v_2(t) = \frac{1}{\tau_2}\int_0^t v_{sc}(t')\ e^{\frac{-(t-t')}{\tau_2}}dt', \quad (5)$$

$$v_3(t) = \frac{1}{\tau_3}\int_0^t v_{sc}(t')\ e^{\frac{-(t-t')}{\tau_3}}dt'. \quad (6)$$

Simplifying (4) into matrix form, $i_{sc} = \mathbf{U}\beta$, the circuit parameters, β=[C_1,C_{var}, $1/R_2$, $1/R_3$]^T, can be estimated as,

$$\widehat{\beta} = \left(\mathbf{U}^T\mathbf{U}\right)^{-1}\mathbf{U}^T i_{sc}. \quad (7)$$

The predictor matrix, $\mathbf{U}$, depends only on v_{sc}, which is observable, and τ_2 and τ_3 which are determined separately,

$$\mathbf{U} = \left[\frac{dv_{sc}}{dt},\ v_{sc}\frac{dv_{sc}}{dt},\ v_{sc} - v_2,\ v_{sc} - v_3\right]. \quad (8)$$

After using LMSE to calculate $\widehat{\beta}$, the remaining circuit parameters are: R_{serial}, C_2, C_3, and R_{leak}. R_{serial} is found by observing the change, ΔV in v_{sc}, that occurs in response to the change, ΔI when i_{sc} is switched off,

$$R_{serial} = \frac{\Delta V}{\Delta I}. \quad (9)$$

The capacitances, C_2 and C_3, are calculated from the time constants,

$$C_2 = \frac{1}{R_2}\tau_2, \text{ and } C_3 = \frac{1}{R_3}\tau_3. \quad (10)$$

The time constants, τ_2 and τ_3, are not estimated by the LMSE procedure, but are needed to calculate, v_2 and v_3 using (5) and (6). As in prior work [15], it is possible to make assumptions that dictate the time scale of each branch. This is comparable to fixing τ_2 and τ_3 heuristically. Alternatively, the LMSE procedure is performed iteratively to search over different values for τ_2 and τ_3 that minimize the mean square error in LMSE. For the iterative search, it is important that the test data for v_{sc} and i_{sc} contain a rich variation of supercapacitor behavior over different time scales. The last parameter, R_{leak}, models long-term leakage, and cannot be observed over a short duration. A fixed value for R_{leak} can be fitted to the observed decline in v_{sc} after redistribution is given enough time to ensure that the supercapacitor is in an equilibrium state. However, the most significant decline in v_{sc} that occurs immediately after charging stops and is well modeled by charge redistribution. Because the impact of leakage on energy awareness is overshadowed by redistribution for harvesting applications, R_{leak} is preset generically based on the manufacturer's specifications.

While calculating $\widehat{\beta}$, it is useful to realize that LMSE penalizes the squared value of the residual error in the fitted current. When the scale of the current into supercapacitor varies by orders of magnitude, it is useful to normalize both i_{sc} and $\mathbf{U}$ by i_{sc}^{-1} so errors at high current do not overshadow all else. LMSE also weights each sample evenly, so downsampling in proportion to i_{sc}^{-1} was found to improve results. This technique devotes equal numbers of samples to each charging test regardless of the actual duration needed for each test current to charge the supercapacitor.

4. Kalman tracking method

Using the three branch equivalent circuit, the supercapacitor's SOC at each time step, t_n, can be represented as a vector of the voltages across each capacitance of the equivalent circuit shown in Fig. 1b,

$$\mathbf{x}_n = [\,v_1(t_n),\quad v_2(t_n),\quad v_3(t_n)\,]^T. \quad (11)$$

Tracking $\mathbf{x}_n$, via the classic Kalman technique (Chap. 13, [36]), relies on the fact that random Gaussian inputs to a linear dynamic system will produce a random Gaussian output. Consequently, the three branch equivalent circuit is modeled as a linear system,

$$\mathbf{x}_n = \mathbf{F}\mathbf{x}_{n-1} + \mathbf{B}\mathbf{u}_n + \mathbf{w}_n, \quad (12)$$

$$\mathbf{z}_n = \mathbf{H}\mathbf{x}_n + \mathbf{D}\mathbf{u}_n + \mathbf{v}_n. \quad (13)$$

Using $\mathcal{N}(\boldsymbol{\mu}, \boldsymbol{\Sigma})$ to represent a multivariate Gaussian distribution with mean, $\boldsymbol{\mu}$, and covariance matrix, $\boldsymbol{\Sigma}$, uncertainty is modeled by the additive white Gaussian noise (AWGN) signals,

$$\mathbf{w}_n \sim \mathcal{N}(0, \mathbf{Q}), \quad (14)$$

$$\mathbf{v}_n \sim \mathcal{N}(0, \mathbf{R}). \quad (15)$$

The assumption of zero means for the noise processes in the formulation is not particularly limiting and the formulation can be extended to address the nonzero mean situations as is standardly done in statistical signal processing.

For the three branch equivalent circuit, the input, $\mathbf{u}_n$, is the average value of i_{sc} into the supercapacitor over the time t_{n-1} to t_n. The output, $\mathbf{z}_n$, is v_{sc} measured at time t_n. The matrices, $\mathbf{F}$, $\mathbf{B}$, $\mathbf{H}$ and $\mathbf{D}$, are found by solving the system of linear ODE (ordinary differential equations) from the three branch equivalent circuit,

$$\frac{d}{dt}\mathbf{x}(t) = \mathbf{F}_\Delta\mathbf{x}(t) + \mathbf{B}_\Delta\mathbf{u}(t), \quad (16)$$

$$\mathbf{z}(t) = \mathbf{H}\mathbf{x}(t) + \mathbf{D}\mathbf{u}(t). \quad (17)$$

The matrices, $\mathbf{F}_\Delta$, $\mathbf{B}_\Delta$, $\mathbf{H}$, and $\mathbf{D}$, are given in Table 1. The solution, $\mathbf{x}_n$, for the system of ODE is a sum of the homogeneous, $\mathbf{x}_{homo}$ and particular solutions, $\mathbf{x}_{part}$,

$$\mathbf{x}_{homo}(t_n) = e^{(t_n - t_{n-1})\mathbf{F}_\Delta}\cdot\mathbf{x}(t_{n-1}), \quad (18)$$

$$\mathbf{x}_{part}(t_n) = \int_{t_{n-1}}^{t_n} e^{(t' - t_{n-1})\mathbf{F}_\Delta}\cdot\mathbf{B}_\Delta\mathbf{u}(t')\ dt', \quad (19)$$

where both (18) and (19) rely on the standard definition of the

Table 1
Parameter matrices for three branch equivalent circuit differential equation system in (16) and (17).

$$\mathbf{F}_\Delta = \begin{bmatrix} \frac{1}{\tau_1}\frac{R_\parallel - R_{\text{serial}}}{R_{\text{serial}}} & \frac{1}{\tau_1}\frac{R_\parallel}{R_2} & \frac{1}{\tau_1}\frac{R_\parallel}{R_3} \\ \frac{1}{\tau_2}\frac{R_\parallel}{R_{\text{serial}}} & \frac{1}{\tau_2}\frac{R_\parallel - R_2}{R_2} & \frac{1}{\tau_2}\frac{R_\parallel}{R_3} \\ \frac{1}{\tau_3}\frac{R_\parallel}{R_{\text{serial}}} & \frac{1}{\tau_3}\frac{R_\parallel}{R_2} & \frac{1}{\tau_3}\frac{R_\parallel - R_3}{R_3} \end{bmatrix}, \quad \mathbf{B}_\Delta = \begin{bmatrix} \frac{1}{\tau_1}R_\parallel \\ \frac{1}{\tau_2}R_\parallel \\ \frac{1}{\tau_3}R_\parallel \end{bmatrix},$$

$$\mathbf{H} = \begin{bmatrix} \frac{R_\parallel}{R_{\text{serial}}} & \frac{R_\parallel}{R_2} & \frac{R_\parallel}{R_3} \end{bmatrix}, \quad \mathbf{D} = [R_\parallel].$$

$$\tau_1 = R_{\text{serial}}(C_1 + C_{\text{var}}v_1), \quad \tau_2 = R_2C_2, \quad \tau_3 = R_3C_3,$$

$$R_\parallel = \left(R_{\text{serial}}^{-1} + R_2^{-1} + R_3^{-1} + R_{\text{leak}}^{-1}\right)^{-1}.$$

matrix exponential, $e^{\mathbf{X}} = \sum_{k=0}^{\infty}\mathbf{X}^k/\mathbf{k}!$. Using (18) and (19) respectively, the transition matrix, $\mathbf{F}$, and input matrix, $\mathbf{B}$, are,

$$\mathbf{F} = e^{(t_n - t_{n-1})\mathbf{F}_\Delta}, \tag{20}$$

$$\mathbf{B} = \mathbf{F}_\Delta^{-1}\left(e^{(t_n - t_{n-1})\mathbf{F}_\Delta} - \mathbf{I}\right)\cdot\mathbf{B}_\Delta. \tag{21}$$

The integral appearing in (19) has been simplified using properties of matrix exponentiation. The output matrices, $\mathbf{H}$ and $\mathbf{D}$, are taken directly from the equivalent circuit as listed in Table 1.

Due to the voltage dependent capacitance, τ_1 in $\mathbf{F}_\Delta$ is not fixed and (16) is not strictly a linear system. However, the variation of τ_1 over the time step from t_{n-1} to t_n is minimal. The approximate linear solution, given by (18) and (19), and referred to as the EKF (extended Kalman filter), provides accurate results. For many other applications that require models with greater non-linearity, the alternative SPKF (sigma point Kalman filter) is needed [37].

The covariance matrices $\mathbf{Q}$ and $\mathbf{R}$ are set heuristically to balance convergence speed against noise tolerance. Specifically, we set $\mathbf{Q}$ and $\mathbf{R}$ as diagonal matrices,

$$\mathbf{Q} = \alpha(|i_{\text{sc}}| + \varepsilon)(t_n - t_{n-1})\begin{bmatrix} \frac{R_\parallel}{\tau_1} & 0 & 0 \\ 0 & \frac{R_\parallel}{\tau_2} & 0 \\ 0 & 0 & \frac{R_\parallel}{\tau_3} \end{bmatrix}, \tag{22}$$

$$\mathbf{R} = \alpha(|i_{\text{sc}}| + \varepsilon)\begin{bmatrix} R_\parallel \end{bmatrix}, \tag{23}$$

where ε is a small value introduced to ensure invertibility and α is the gain factor. Intuitively, (22) assumes an uncertainty in each predicted state variable that is roughly proportional to the magnitude of its change between adjacent observations; and (23) assumes an uncertainty in the predicted output that is roughly proportional to the magnitude of the resistive voltage drop due to the input current. Values of $\varepsilon = 0.01$ and $\alpha = 0.01$ were used and the method was not found to be particularly sensitive to variations in these parameters.

For each time step, t_n, Kalman filtering calculates the MAP (maximum a posteriori) estimate of the state, $\hat{\mathbf{x}}_n$, and its error covariance matrix, $\hat{\mathbf{P}}_n$,

$$\hat{\mathbf{x}}_n = \tilde{\mathbf{x}}_n + \mathbf{K}(\mathbf{z}_n - \mathbf{H}\tilde{\mathbf{x}}_n - \mathbf{D}\mathbf{u}_n), \tag{24}$$

$$\hat{\mathbf{P}}_n = \tilde{\mathbf{P}}_n - \mathbf{K}\mathbf{H}\tilde{\mathbf{P}}_n, \tag{25}$$

where the Kalman gain, $\mathbf{K}$, is,

$$\mathbf{K} = \tilde{\mathbf{P}}_n\mathbf{H}^{\text{T}}\left(\mathbf{H}\tilde{\mathbf{P}}_n\mathbf{H}^{\text{T}} + \mathbf{R}\right)^{-1}, \tag{26}$$

and the mean, $\tilde{\mathbf{x}}_n$ and covariance, $\tilde{\mathbf{P}}_n$, of the predicted prior distribution for $\mathbf{x}_n$ are calculated as,

$$\tilde{\mathbf{x}}_n = \mathbf{F}\hat{\mathbf{x}}_{n-1} + \mathbf{B}\mathbf{u}_n, \tag{27}$$

$$\tilde{\mathbf{P}}_n = \mathbf{F}\hat{\mathbf{P}}_{n-1}\mathbf{F}^{\text{T}} + \mathbf{Q}. \tag{28}$$

A quick discussion of these Kalman equations is given in Section 8 in the Supplementary material.

5. Evaluation method

Evaluation demonstrates how both of the proposed methods, parameter estimation and Kalman tracking, each improve energy awareness. Performance is characterized by the error between the models' predictions and the actual observed energy that would be available to an application.

As a baseline, the stored energy in a supercapacitor is predicted from v_{sc} using the simple capacitive model,

$$E = \frac{1}{2}C_{\text{simple}}v_{\text{sc}}^2. \tag{29}$$

Alternatively, E is predicted from a supercapacitor's SOC using the three branch equivalent circuit model,

$$E = \frac{1}{2}C_1v_1^2 + \frac{1}{3}C_{\text{var}}v_1^3 + \frac{1}{2}C_2v_2^2 + \frac{1}{2}C_3v_3^2. \tag{30}$$

Intuitively, (29) and (30) can be validated by measuring the total energy that is recovered by completely discharging a supercapacitor. However, long-term charge storage in a supercapacitor may still hold significant energy even after v_{sc} is discharged to zero volts. This unaccounted-for energy complicates validating E directly.

Rather than completely discharging a supercapacitor, energy awareness is validated by predicting the change in a supercapacitor's stored energy, ΔE, while a supercapacitor is charged and discharged to various given final voltages. This corresponds to predicting how much energy would be available to an application before v_{sc} falls below a minimum operating voltage. Additionally the three branch equivalent circuit predicts internal losses, W, by integrating the power dissipated from each of the model's resistors. The simple model of (29) does not include internal losses. The observed energy, E_{obs}, that can be accurately measured is predicted by the model as,

$$E_{\text{obs}} = \Delta E + W. \tag{31}$$

Both the proposed methods and the simple capacitive model are tested by estimating ΔE over durations of constant current charging ($\Delta E > 0$) and discharging ($\Delta E < 0$), and durations of redistribution where i_{sc} is zero. First, the proposed Kalman tracking method estimates the initial SOC. Starting at this initial SOC, Equations (12) and (13) are then used to predict the supercapacitor's behavior until v_{sc} reaches the same final voltage as the observed data. Finally, Equations (29) and (30) are used to predict E before and after the duration of constant current. The change in stored energy, ΔE, is compared against the observed energy,

$$\text{error} = E_{\text{obs}} - (\Delta E + W). \tag{32}$$

In order to validate parameter estimation, the supercapacitor is charged from a known completely discharged state, such that there

is no need to use tracking to estimate the initial state. Before each test the supercapacitor is discharged and then left overnight with its terminals short circuited. Because the initial E is zero, E_{obs} can be directly compared to the stored energy, E.

6. Results and discussion

The experimental setup for charging and discharging the supercapacitors is shown in Fig. 4. Testing is conducted for 5 F, 50 F, and 350 F *Maxwell BoostCap* supercapacitors [38], and a 10 F device from *Illinois Capacitor* [39]. The range of charging currents for the 50 F supercapacitor is set to coincide with the variability range of solar energy harvesting shown in Fig. 3. Charging currents are supplied by a *Nemic-Lambda ZUP (36 V-24 A)* current source. The supercapacitor's terminal voltage is measured using an ADC (analog to digital converter) on a *Microchip PIC16F1783* PIC (programmable interface controller). The PIC also automatically controls the timing. A power MOSFET allows the PIC to disconnect the charging current when the supercapacitor reaches its rated voltage. Discharging the supercapacitor is done by a *TekPower 3710A DC Electronic Load (0-360 V/150 W)* in constant current mode. The PIC controls a second MOSFET that disconnects the load when v_{sc} falls below .35 V because the constant load current becomes unreliable below that point.

6.1. Parameter estimation

Because the true parameters of a physical supercapacitor are not accessible, parameter estimation is first tested using simulated data rather than observed data. Using known parameters from prior work [15], Equations (12) and (13) simulate the SOC and v_{sc} of a 470 F DLC supercapacitor as it is charged from a completely discharged state to its rated voltage (2.3 V). Three different constant currents are used to charge the supercapacitor at approximately 5%, .5%, and .05% of its listed short circuit current. Using the simulated i_{sc} and v_{sc} data, Equations (7) and (8) are able to accurately recover the true parameters used to generate the simulated data. Table 2 shows the accuracy of the estimated parameters. The proposed LMSE method is able to improve on the accuracy of the prior parameter estimation method [15] because it does not rely on the assumption that significant current only flows into one branch of the circuit at a time. This allows the proposed method to more accurately distinguish the simultaneous effects of charge redistribution and voltage dependent capacitance. Consequently, the proposed parameter estimation improves the accuracy of both C_{var} and the parameters of the second and third branches. The average deviation between the fitted parameters and the simulation groundtruth is decreased from 13% error for the method of [15] to less than 2% error for the proposed method.

Table 2
The proposed (LMSE fit) technique is compared to prior work (Ref. [15] fit) for estimating the parameters of the three branch equivalent circuit. The parameters are estimated using simulated measurement data for a 470 F DLC with (true) parameters specified in Ref. [15].

	470 F DLC (simulation)		
	Truth	LMSE fit	Ref. [15] fit
C_1	270 F	273 F	278 F
C_{var}	190 F/V	191 F/V	200 F/V
R_{serial}	2.5 mΩ	2.5 mΩ	2.5 mΩ
C_2	100 F	98 F	138 F
R_2	.90 Ω	.92 Ω	.87 Ω
C_3	220 F	231 F	143 F
R_3	5.2 Ω	5.2 Ω	5.5 Ω
R_{leak}	8 kΩ	Fitted separately [15]	

In terms of energy awareness for physical supercapacitors, the benefits of the three branch equivalent circuit model are shown in Fig. 5. Parameters for the 5 F, 10 F, 50 F, and 350 F supercapacitors are estimated using the procedure given in Section 3. The required input data, i_{sc} and v_{sc}, is a concatenation of 10 mA, 100 mA, and 1 A charging patterns for the 10 F supercapacitor; 100 mA, 1 A, and 10 A charging patterns shown in Fig. 6 for the 50F supercapacitor; and 500 mA, 2 A, 10 A, and 20 A charging patterns for the 350 F supercapacitor. Additionally, a 70 A charging behavior is modeled for the 350 F, but observed data was not collected for that current. The fitted parameters are given in Table 3, and used to estimate ΔE and W in Fig. 5. In order to test the reliability of the proposed parameter estimation, multiple 50 F supercapacitors are tested. As shown in Table S1 in the supplementary material, the fitted parameters across multiple 50 F devices are consistent within a reasonable tolerance that is expected for physical devices.

As compared to using the rated capacitance, C_{rated}, to predict the stored energy, the three branch equivalent circuit is able to account for the varying behavior of the supercapacitors at different charging currents. Even when the simple capacitance, C_{simple}, is fitted using the same charging data, a fixed capacitance underestimates E at low currents when a greater portion of the charge storage on the supercapacitor's porous electrode surfaces is utilized, and overestimates E at high current when a smaller portion is utilized. The simple capacitive models are also unable to model the energy, W, that is dissipated internally as waste. Neglecting W causes the simple capacitive model to consistently underestimate E even

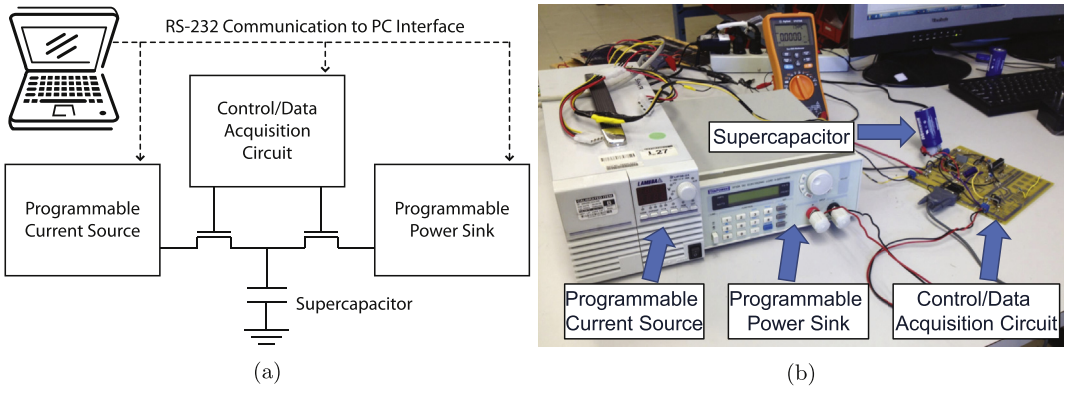

Fig. 4. The validation setup depicted in (a) uses a PIC microcontroller to control the charging and discharging currents via MOSFET gates. Data logging and high level control of each module is done from a workstation running Matlab via RS-232 serial connections. The corresponding arrangement of the test equipment is pictured in (b), showing a 350 F supercapacitor.

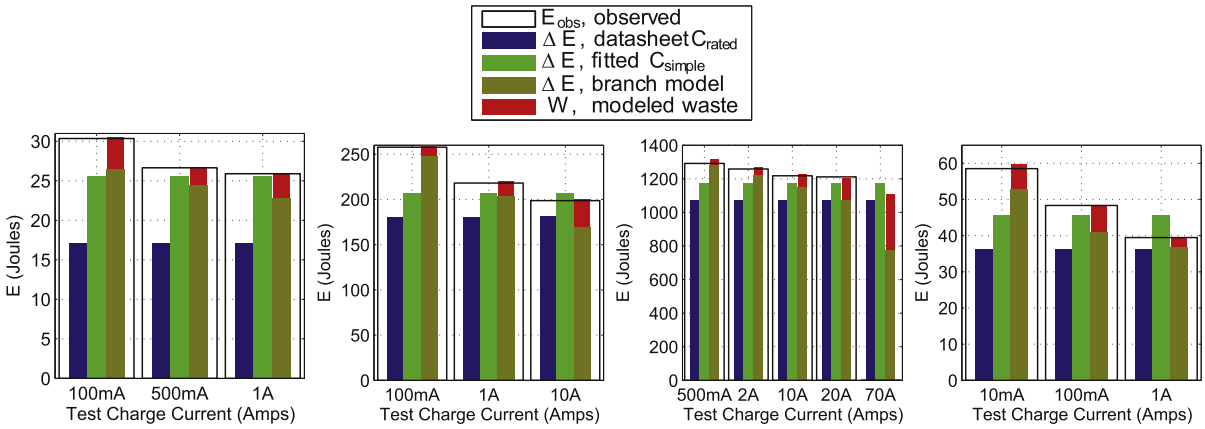

(a) 5F (b) 50F (c) 350F (d) 10F

Fig. 5. The energy (E_{obs}, observed) that is required to charge the supercapacitor from rest to its rated voltage depends on the charging current. Three techniques for predicting E_{obs} are compared. The first two techniques (datasheet C_{rated}) and (fitted C_{simple}) used a fixed capacitance. Alternatively, the three branch equivalent circuit (branch model) is used to predict both the stored energy, ΔE, and internal losses, W. Results for the Maxwell supercapacitors are shown in (a), (b), and (c), while (d) shows the results for the Illinois Capacitor device.

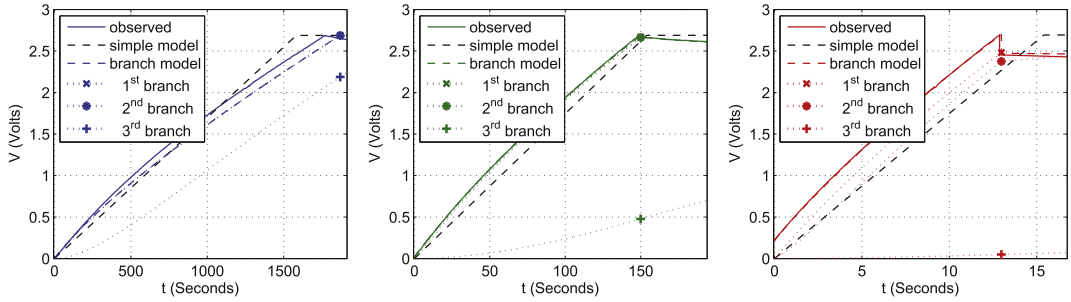

(a) 100mA charging. (b) 1A charging. (c) 10A charging.

Fig. 6. These 100 mA, 1 A and 10 A charging tests for the 50 F supercapacitor in (a), (b), and (c), provide the (observed) data used to fit the parameters. The resulting parameters for the three branch equivalent circuit (branch model) and simple capacitive (simple model) are then simulated in order to predict the duration and energy that are required to charge the supercapacitor from a completely discharged state to its rated voltage (2.7 V) at each current.

Table 3
The propose LMSE technique is used to estimate the parameters of the 5 F, 10 F, 50 F, and 350 F supercapacitors using observed training data.

	IL Cap [39]	Maxwell BCAP [38]		
C_{rated}	10 F	5 F	50 F	350 F
C_{simple}	13 F	7.5 F	57 F	383 F
C_1	8.8 F	5.2 F	40 F	264 F
C_{var}	.63 F/V	1.0 F/V	9.1 F/V	50 F/V
R_{serial}	39 mΩ	110 mΩ	22 mΩ	6.4 mΩ
C_2	.84 F	.68 F	2.2 F	51 F
R_2	8.1 Ω	10 Ω	3.0 Ω	.13 Ω
C_3	6.0 F	4.4 F	11 F	33 F
R_3	79 Ω	110 Ω	43 Ω	14 Ω
R_{leak}	90 kΩ	180 kΩ	36 kΩ	9 kΩ

when C_{simple} is fitted to dv_{sc}/dt. Cross-validation of the three branch equivalent circuit's ability to model E for data not used for fitting is shown next for the SOC tracking technique.

6.2. Kalman tracking

The energy awareness benefits of proposed Kalman methods are validated by tracking a supercapacitor's SOC as it is repeatedly charged and discharged. Because the supercapacitor is no longer in a known completely discharged state at the start of each charge cycle, the proposed Kalman tracking technique is used to track the SOC, as shown in Fig. 7. The exception is the very first 5 A charging current where the supercapacitor starts from rest.

Using the estimated SOC at the start of each duration of charging, discharging and redistribution, the three branch equivalent circuit predicts ΔE that is transferred to or from the supercapacitor. Fig. 8 compares the estimates of ΔE and W against the observed energy E_{obs}. Using the three branch equivalent circuit model outperforms the simple models that use either the fixed capacitance, C_{rated}, from the datasheet, or C_{simple}, fitted to the observed data. The fixed capacitive models for energy awareness especially struggle during redistribution when i_{sc} is zero. These models cannot account for the decrease in v_{sc} unaccompanied by energy output during redistribution. At each point where the supercapacitor is maximally charged, the estimated energy available to an application would be subject to both the error during redistribution and discharging, for a total overestimation of up to 18 J by the simple model. The maximum total error for the Kalman tracking is 5.8 J. As shown in the results for parameter estimation, the spontaneous decrease in v_{sc} is best modeled by the three branch equivalent circuit as opposed to more complex leakage models. Leakage models would have greater difficulty accounting for the systematic error of the simple capacitive model during the charging cycles that is well explained by the three branch equivalent circuit.

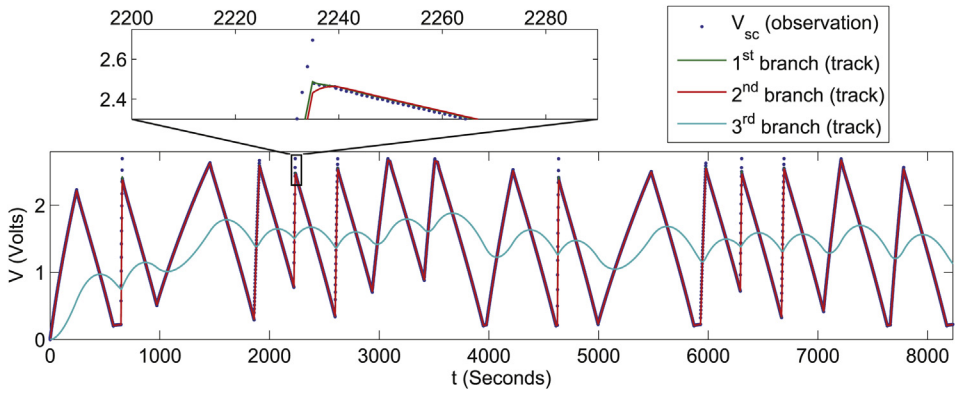

Fig. 7. The proposed Kalman technique for tracking the 50 F supercapacitor's internal SOC is experimentally validated over a series of various charging currents designed to show the range of possible solar variability from Fig. 3. The top, zoomed, axes show the much shorter time scale of the 1st and 2nd branch voltages.

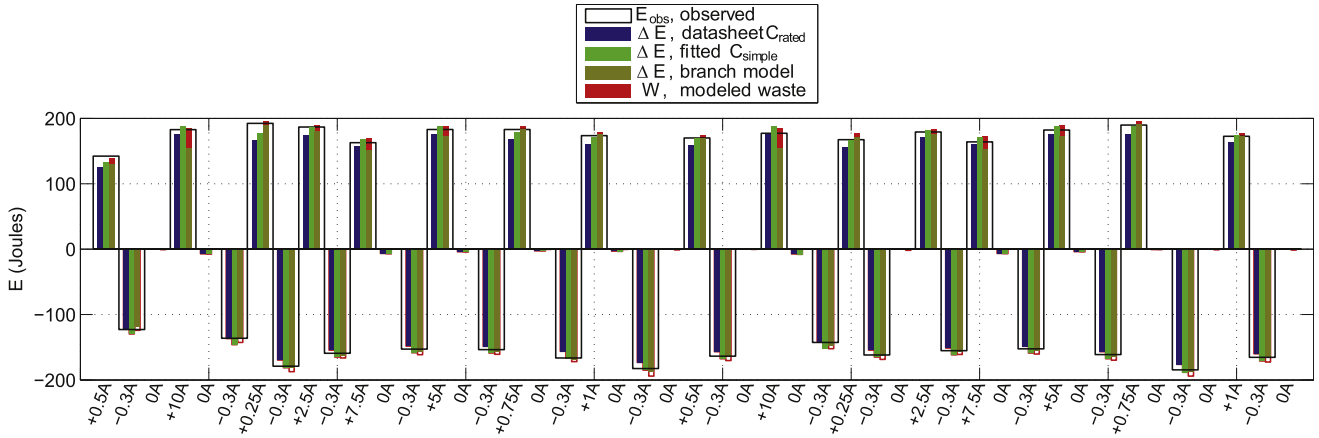

Fig. 8. For each charging (>0 A), redistribution (0 A), and discharging (<0 A) duration of the tracking experiment shown in Fig. 7, the energy transfer, E_{obs} (observed), is predicted using both models: the (branch model) and the fixed capacitive models using C_{rated} (datasheet) from the manufacturer, and C_{simple} (fitted) from the training data. The RMS (root mean squared) error is 3.8 J for the branch model, compared to 5.5 J and 8.3 J for the respective fitted and datasheet fixed capacitive models. Corresponding numeric data is given in the supplementary material in Table S2.

7. Conclusions

This paper has provided a novel technique to monitor the remaining energy stored in a supercapacitor by tracking its SOC using the three branch equivalent circuit model in conjunction with a Kalman tracker. Tracking a supercapacitor's SOC is shown to reduce the error in estimation of the net change in the buffered energy, ΔE_{tot} by 67% and 49% as compared to the simple capacitive model using the datasheet and fitting respectively to set C_{simple}. It is shown that charge redistribution is the main source of the simple model's inaccuracy, justifying the use of the three branch equivalent circuit to model the supercapacitor's SOC. With an eye towards applicability, a novel parameter estimation technique is also proposed such that the parameters of the three branch circuit can be calculated from arbitrary current and voltage profiles observed while the supercapacitor operates normally in its application setting. The two significant benefits of this on-line parameter estimation are: 1) there is no need to take device off-line to measure the parameters or possible degradation of capacity over time, or perform specific tests before individual systems are deployed to account for variation in capacity due to manufacturing tolerances; 2) on-line parameter estimation allows the model to be fitted to the same data it is tracking such that any biased measurements due to hardware on a specific system will be incorporated into the parameters. The performance of both proposed techniques, parameter estimation and SOC tracking, are physically validated for 5 F, 10 F, 50 F and 350 F supercapacitors and shown to outperform the simple capacitive model for supercapacitor behavior.

Appendix A. Supplementary data

Supplementary data related to this article can be found at http://dx.doi.org/10.1016/j.jpowsour.2015.07.050.

References

[1] A. Nadeau, G. Sharma, T. Soyata, State-of-charge estimation for supercapacitors: a Kalman filtering formulation, in: Proc. IEEE Intl. Conf. Acoustics Speech and Sig. Proc., ICASSP, Florence, Italy, 2014, pp. 2194–2198, http://dx.doi.org/10.1109/ICASSP.2014.6853988.

[2] P. Simon, Y. Gogotsi, B. Dunn, Where do batteries end and supercapacitors begin? Sci. Mag. 343 (2014) 1210–1211, http://dx.doi.org/10.1126/science.1249625.

[3] A. Gee, F. Robinson, R. Dunn, Analysis of battery lifetime extension in a small-scale wind-energy system using supercapacitors, IEEE Trans. Energy Convers. 28 (1) (2013) 24–33, http://dx.doi.org/10.1109/TEC.2012.2228195.

[4] S. Lukic, S. Wirasingha, F. Rodriguez, J. Cao, A. Emadi, Power management of an ultracapacitor/battery hybrid energy storage system in an HEV, IEEE Veh. Power Propuls. Conf. (VPPC) (2006) 1–6, http://dx.doi.org/10.1109/VPPC.2006.364357.

[5] H. Jia, Y. Mu, Y. Qi, A statistical model to determine the capacity of batter-ysupercapacitor hybrid energy storage system in autonomous microgrid, Int. J. Electr. Power Energy Syst. 54 (0) (2014) 516–524. http://dx.doi.org/10.1016/j.ijepes.2013.07.025.

[6] J. Dixon, M. Ortuzar, Ultracapacitors + DC–DC converters in regenerative braking system, IEEE Aerosp. Electron. Sys. Mag. 17 (8) (2002) 16–21, http://dx.doi.org/10.1109/MAES.2002.1028079.
[7] J.P. Torreglosa, P. Garcia, L.M. Fernandez, F. Jurado, Predictive control for the energy management of a fuel-cell–battery–supercapacitor tramway, IEEE Trans. Ind. Inf. 10 (1) (2014) 276–285, http://dx.doi.org/10.1109/TII.2013.2245140.
[8] Q. Li, W. Chen, Z. Liu, M. Li, L. Ma, Development of energy management system based on a power sharing strategy for a fuel cell-battery-supercapacitor hybrid tramway, J. Power Sources 279 (2015) 267–280, http://dx.doi.org/10.1016/j.jpowsour.2014.12.042, 9th International Conference on Lead-Acid Batteries {LABAT} 2014.
[9] A. Fahad, T. Soyata, T. Wang, G. Sharma, W. Heinzelman, K. Shen, SOLARCAP: super capacitor buffering of solar energy for self-sustainable field systems, in: Proceedings of the 25th IEEE International System-on-chip Conference (IEEE SOCC), Niagara Falls, NY, 2012, pp. 236–241, http://dx.doi.org/10.1109/SOCC.2012.6398354.
[10] M. Hassanalieragh, T. Soyata, A. Nadeau, G. Sharma, Solar-supercapacitor harvesting system design for energy-aware applications, in: Proceedings of the 27th IEEE International System-on-chip Conference (IEEE SOCC), Las Vegas, NV, 2014, pp. 280–285, http://dx.doi.org/10.1109/SOCC.2014.6948941.
[11] F.I. Simjee, P.H. Chou, Efficient charging of supercapacitors for extended lifetime of wireless sensor nodes, IEEE Trans. Power Electron. 23 (3) (2008) 1526–1536, http://dx.doi.org/10.1109/TPEL.2008.921078.
[12] D. Linzen, S. Buller, E. Karden, R.W. De Doncker, Analysis and evaluation of charge-balancing circuits on performance, reliability, and lifetime of supercapacitor systems, IEEE Trans. Ind. Appl. 41 (5) (2005) 1135–1141, http://dx.doi.org/10.1109/TIA.2005.853375.
[13] B. Conway, V. Birss, J. Wojtowicz, The role and utilization of pseudocapacitance for energy storage by supercapacitors, J. Power Sources 66 (1–2) (1997) 1–14, http://dx.doi.org/10.1016/S0378-7753(96)02474-3.
[14] N. Bertrand, J. Sabatier, O. Briat, J.-M. Vinassa, Embedded fractional nonlinear supercapacitor model and its parametric estimation method, IEEE Trans. Ind. Appl. 57 (12) (2010) 3991–4000, http://dx.doi.org/10.1109/TIE.2010.2076307.
[15] L. Zubieta, R. Bonert, Characterization of double-layer capacitors for power electronics applications, IEEE Trans. Ind. Appl. 36 (1) (2000) 199–205, http://dx.doi.org/10.1109/28.821816.
[16] J. Niu, W.G. Pell, B.E. Conway, Requirements for performance characterization of c double-layer supercapacitors: applications to a high specific-area c-cloth material, J. Power Sources 156 (2) (2006) 725–740, http://dx.doi.org/10.1016/j.jpowsour.2005.06.002.
[17] Y. Zhang, H. Yang, Modeling and characterization of supercapacitors for wireless sensor network applications, J. Power Sources 196 (8) (2011) 4128–4135, http://dx.doi.org/10.1016/j.jpowsour.2010.11.152.
[18] H. Yang, Y. Zhang, Self-discharge analysis and characterization of supercapacitors for environmentally powered wireless sensor network applications, J. Power Sources 196 (20) (2011) 8866–8873, http://dx.doi.org/10.1016/j.jpowsour.2011.06.042.
[19] N. Devillers, S. Jemei, M.-C. Pra, D. Bienaim, F. Gustin, Review of characterization methods for supercapacitor modelling, J. Power Sources 246 (2014) 596–608. http://dx.doi.org/10.1016/j.jpowsour.2013.07.116.
[20] V. Sedlakova, J. Sikula, J. Majzner, P. Sedlak, T. Kuparowitz, B. Buergler, P. Vasina, Supercapacitor equivalent electrical circuit model based on charges redistribution by diffusion, J. Power Sources 286 (2015) 58–65, http://dx.doi.org/10.1016/j.jpowsour.2015.03.122.
[21] D. Torregrossa, M. Bahramipanah, E. Namor, R. Cherkaoui, M. Paolone, Improvement of dynamic modeling of supercapacitor by residual charge effect estimation, IEEE Trans. Ind. Appl. 61 (3) (2014) 1345–1354, http://dx.doi.org/10.1109/TIE.2013.2259780.
[22] S. Buller, E. Karden, D. Kok, R. De Doncker, Modeling the dynamic behavior of supercapacitors using impedance spectroscopy, IEEE Trans. Ind. Appl. 38 (6) (2002) 1622–1626, http://dx.doi.org/10.1109/TIA.2002.804762.
[23] S. Buller, M. Thele, R. De Doncker, E. Karden, Impedance-based simulation models of supercapacitors and Li-ion batteries for power electronic applications, IEEE Trans. Ind. Appl. 41 (3) (2005) 742–747, http://dx.doi.org/10.1109/TIA.2005.847280.
[24] F. Rafik, H. Gualous, R. Gallay, A. Crausaz, A. Berthon, Frequency, thermal and voltage supercapacitor characterization and modeling, J. Power Sources 165 (2) (2007) 928–934, http://dx.doi.org/10.1016/j.jpowsour.2006.12.021.
[25] A. Oukaour, M. Pouliquen, B. Tala-Ighil, H. Gualous, E. Pigeon, O. Gehan, B. Boudart, Supercapacitors aging diagnosis using least square algorithm, Microelectron. Reliab. 53 (9) (2013) 1638–1642, http://dx.doi.org/10.1016/j.microrel.2013.07.032.
[26] Y. Diab, P. Venet, H. Gualous, G. Rojat, Self-discharge characterization and modeling of electrochemical capacitor used for power electronics applications, IEEE Trans. Power Electron. 24 (2) (2009) 510–517, http://dx.doi.org/10.1109/TPEL.2008.2007116.
[27] H. Yang, Y. Zhang, Analysis of supercapacitor energy loss for power management in environmentally powered wireless sensor nodes, IEEE Trans. Power Electron. 28 (11) (2013) 5391–5403, http://dx.doi.org/10.1109/TPEL.2013.2238683.
[28] C. Renner, V. Turau, CapLibrate: self-calibration of an energy harvesting power supply with supercapacitors, in: 23rd Intl. Conf. on Architecture of Computing Systems (ARCS), VDE, 2010, pp. 1–10.
[29] C. Renner, V. Turau, State-of-charge assessment for supercap-powered sensor nodes: keep it simple stupid!, in: IEEE Ninth Intl. Conf. on Networked Sensing Systems (INSS), 2012, pp. 1–6, http://dx.doi.org/10.1109/INSS.2012.6240582.
[30] A. Eddahech, M. Ayadi, O. Briat, J.-M. Vinassa, Online parameter identification for real-time supercapacitor performance estimation in automotive applications, Int. J. Electr. Power Energy Syst. 51 (0) (2013) 162–167, http://dx.doi.org/10.1016/j.ijepes.2013.03.001.
[31] V. Johnson, Battery performance models in ADVISOR, J. Power Sources 110 (2) (2002) 321–329.
[32] T. Markel, A. Brooker, T. Hendricks, V. Johnson, K. Kelly, B. Kramer, M. OKeefe, S. Sprik, K. Wipke, Advisor: a systems analysis tool for advanced vehicle modeling, J. Power Sources 110 (2) (2002) 255–266, http://dx.doi.org/10.1016/S0378-7753(02)00189-1.
[33] S. Buller, E. Karden, D. Kok, R. De Doncker, Modeling the dynamic behavior of supercapacitors using impedance spectroscopy, in: Industry Applications Conference, Thirty-sixth IAS Annual Meeting, Vol. 4, 2001, pp. 2500–2504, http://dx.doi.org/10.1109/IAS.2001.955972.
[34] A.S. Weddell, G.V. Merrett, T.J. Kazmierski, B.M. Al-Hashimi, Accurate supercapacitor modeling for energy harvesting wireless sensor nodes, IEEE Trans. Circuits Syst. II Exp. Briefs 58 (12) (2011) 911–915, http://dx.doi.org/10.1109/TCSII.2011.2172712.
[35] R. Faranda, S. Leva, Energy comparison of MPPT techniques for PV systems, WSEAS Trans. Power Syst. 3 (6) (2008) 446–455.
[36] C.M. Bishop, Pattern Recognition and Machine Learning, Information Science and Statistics, Springer, New York, NY, 2006.
[37] R. Van der Merwe, E.A. Wan, The square-root unscented Kalman filter for state and parameter-estimation, in: Proc. IEEE Intl. Conf. on Acoustics, Speech, and Sig, Proc., Vol. 6, ICASSP, 2001, pp. 3461–3464, http://dx.doi.org/10.1109/ICASSP.2001.940586.
[38] Maxwell Technologies, HC Series Ultracapacitors, 2015. www.maxwell.com/images/documents/hcseries_ds_1013793-9.pdf.
[39] Illinois Capacitor Inc, DCN Supercapacitors, 2015. www.illinoiscapacitor.com/pdf/seriesDocuments/DCNseries.pdf.